Supporting Information for

Halogenated Thiophene Serve as Solvent Additives in Mediating Morphology and Reaching Efficient Organic Solar Cells

Lingzhi Guo,[†] Qingduan Li,[†] Jiaxuan Ren,[†] Yuanjie Xu,[†] Jiabin Zhang,[‡] Kai Zhang,[‡] Yuepeng Cai,[†] Shengjian Liu[†], Fei Huang[‡]*

L. Guo, Dr. Q. Li, Dr. J. Ren, Y. Xu, Prof. Y.-P. Cai, and Prof. S. Liu
School of Chemistry, Guangzhou Key Laboratory of Materials for Energy Conversion and Storage, Guangdong Provincial Engineering Technology Research Center for Materials for Energy Conversion and Storage
South China Normal University (SCNU)
Guangzhou 510006, P. R. China
E-mail: shengjian.liu@m.scnu.edu.cn

J. Zhang, Prof. K. Zhang, Prof. F. Huang
Institute of Polymer Optoelectronic Materials and Devices, State Key Laboratory of Luminescent Materials and Devices
South China University of Technology (SCUT)
Guangzhou 510640, P. R. China

Keywords: organic solar cells, halogenated thiophene, solvent additives, morphology, bulk heterojunction

Content

1. Materials

Solvents including chloroform (CF), 1-chloronaphthalene (CN), and 1,8-diiodooctane (DIO) were purchased from commercial sources (Aldrich, Alfa Aesar) and used without further purification unless stated otherwise. The hole transporting materials (2-(9H-carbazol-9-yl)ethyl)phosphonic acid (2PACz) and cathode interface materials 2,9-bis(3-((3-(dimethylamino)propyl)amino)propyl)anthra[2,1,9-def:6,5,10-d'e'f']diisoquinoline-1,3,8,10(2H,9H)-tetraone (PDINN) shown in Figure S1 were purchased from Derthon Co. LTD (Shenzhen, China). The polymer donor poly[(2,6-(4,8-bis(5-(2-ethylhexyl)-4-fluorothiophen-2-yl)benzo[1,2-b:4,5-b0]dithiophene))-co-(1,3-di(5-thiophene-2-yl)-5,7-bis(2-ethylhexyl)-benzo[1,2-c:4,5-c0]dithiophene-4,8-dione))] (PM6), small molecule acceptor 2,2'-((2Z,2'Z)-((12,13-bis(2-ethylhexyl)-3,9-diundecyl-12,13-dihydro-[1]thiadiazolo[3,4-]thieno[2",3":4',5']thieno[2',3':4,5]pyrrolo[3,2-]thieno[2',3':4,5]thieno[3,2-b]indole-2,10-diyl)bis(methanylylidene))bis(5,6-difluoro-3-oxo-2,3-dihydro-1H-indene-2,1-diylidene))dimalononitrile (Y6), 2,2'-((2Z,2'Z)-((3,9-bis(2-butylundecyl)-12,13-bis(2-ethylhexyl)-12,13-dihydro-[1,2,5]thiadiazolo[3,4-e]thieno[2",3":4',5']thieno[2',3':4,5]pyrrolo[3,2-g]thieno[2',3':4,5]thieno[3,2-b]indole-2,10-diyl)bis(methaneylylidene))bis(5,6-difluoro-3-oxo-2,3-dihydro-1H-indene-2,1-diylidene))dimalononitrile (L8-BO), 2,2'-((2Z,2'Z)-((12,13-bis(2-ethylhexyl)-3,9-diundecyl-12,13-dihydro-[1,2,5]thiadiazolo[3,4-e]thieno[2",3":4',5']thieno[2',3':4,5]pyrrolo[3,2-g]thieno[2',3':4,5]thieno[3,2-b]indole-2,10-diyl)bis(methaneylylidene))bis(5,6-dichloro-3-oxo-2,3-dihydro-1H-indene-2,1-diylidene))dimalononitrile (Y6-BO), and 2,2'-((2Z,2'Z)-((12,13-bis(2-butyloctyl)-3,9-diundecyl-12,13-dihydro-[1,2,5]thiadiazolo[3,4-e]thieno[2",3":4',5']thieno[2',3':4,5]pyrrolo[3,2-g]thieno[2',3':4,5]thieno[3,2-b]indole-2,10-diyl)bis(methaneylylidene))bis(5,6-difluoro-3-oxo-2,3-dihydro-1H-indene-2,1-diylidene))dimalononitrile (BTP-eC9) were purchased from Shanghai Vizuchem and Derthon Co. LTD (Shenzhen, China), respectively. The solvent additive 2,5-dibromothiophene (HBrT) was purchased from Shanghai McLean Biochemical

Technology Co. LTD. The new designed solvent additive 2,5-dibromo-3,4-difluoro-thiophene (FBrT) was prepared according to our reported procedure.[1] Scheme 1 outlines the key steps in the synthesis of the FBrT. The ^{1}H NMR, ^{13}C NMR, and ^{19}F NMR of FBrT in $CDCl_3$ were provided in Figure S20-S22.

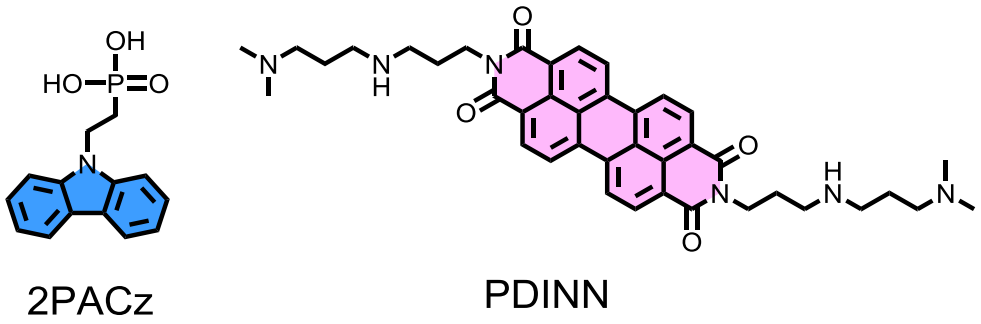

Figure S1. The chemical structures of hole transporting material 2PACz and cathode interface material PDINN.

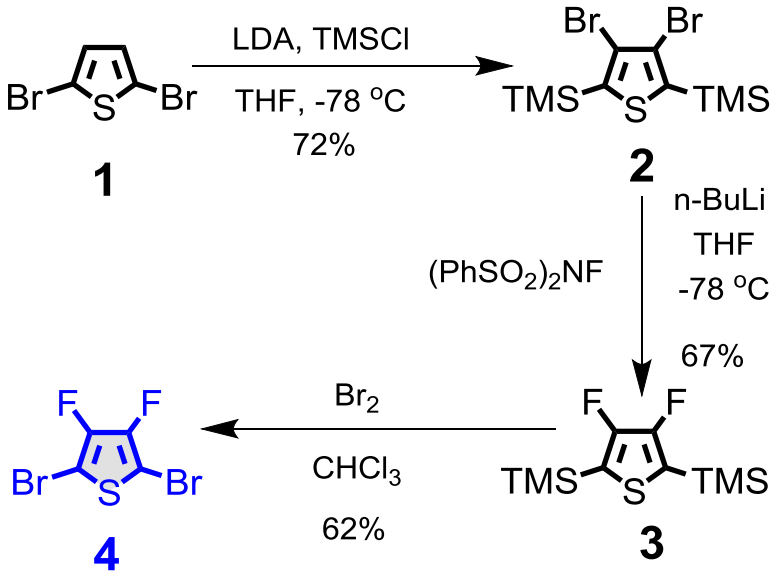

Scheme S1. Synthesis of the new designed solvent additive 2,5-dibromo-3,4-difluoro-thiophene (FBrT).

2. Materials Solubility in Different Solvent Additives

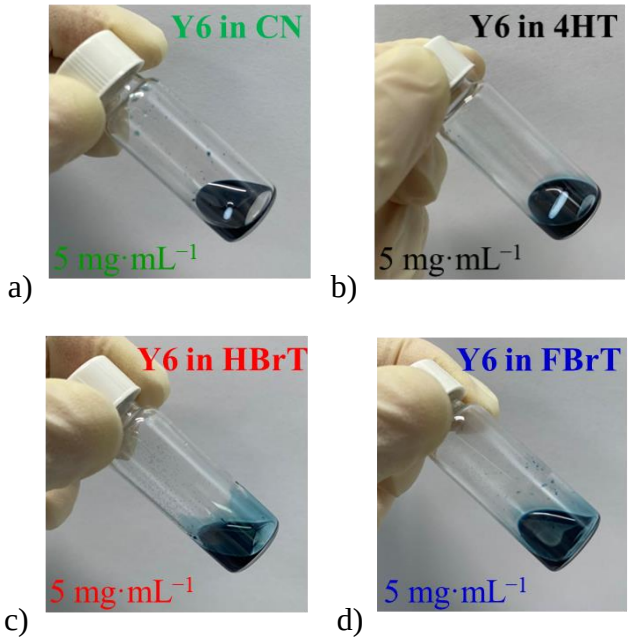

Figure S2. The solubility test of the small molecule acceptor Y6 in (a) CN, (b) 4HT, (c) HBrT, and (d) FBrT solvent additives.

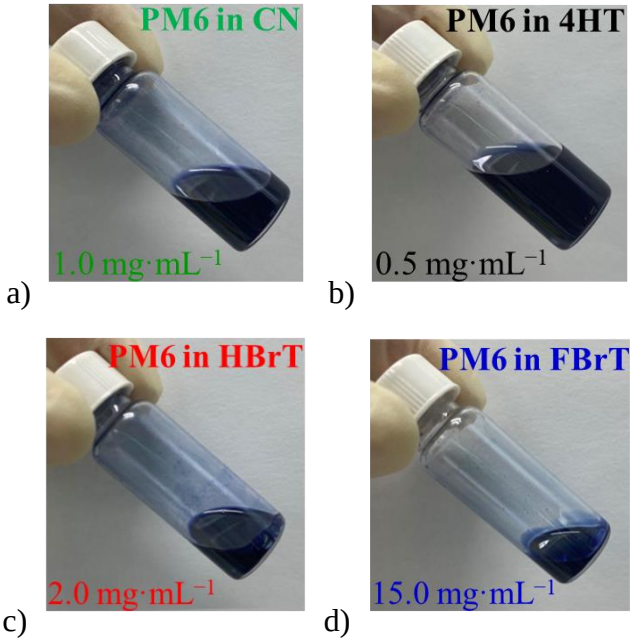

Figure S3. The solubility test of the polymer donor PM6 in (a) CN, (b) 4HT, (c) HBrT, and (d) FBrT solvent additives.

3. UV-Vis Solution-Film Spectroscopy

The UV-vis absorption spectra of the neat PM6 film, neat Y6 film, and BHJ blend films were obtained on a SHIMADZU UV-3600 spectrophotometer. The sample films for UV-vis absorption measurements were prepared on quartz substrates. The thickness of films was determined using a KLA Tencor P6 surface profilometer. The neat films were prepared by dissolving PM6 (5 mg·mL^{-1}) and Y6 (8 mg·mL^{-1}) in CF solvent and adding 0.5 vol% of different additives (FBrT, HBrT, and CN) respectively. The BHJ blend films were prepared by dissolving PM6:Y6 (1:1.2, wt/wt) in CF solvent and adding 0.5 vol% of different additives (FBrT, HBrT, and CN) respectively, and the total concentration of the blend solution was 16 mg·mL^{-1}. After 3 hours of full dissolution, it was spin-coated onto a quartz glass plate, and the neat films and BHJ blend films were tested for UV-vis absorption and thickness.

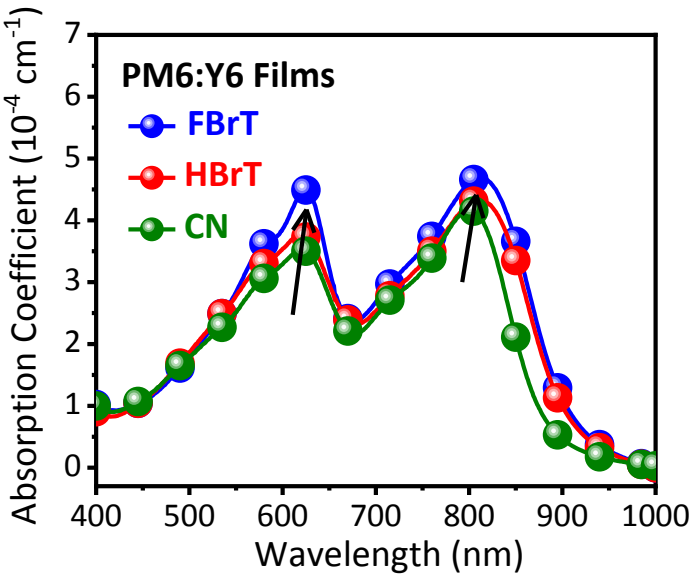

Figure S4. UV-vis absorption spectra of PM6:Y6 BHJ blend films with different solvent additives.

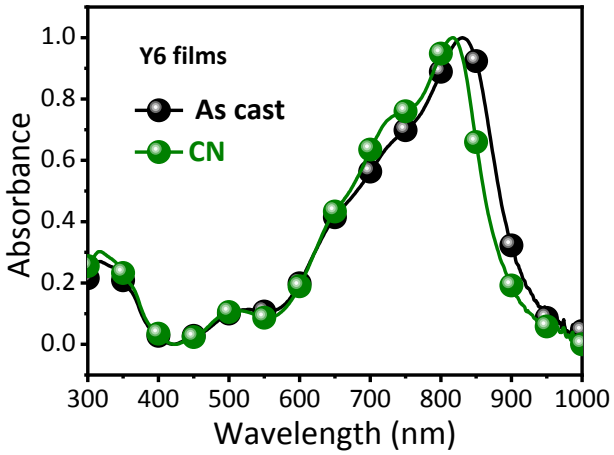

Figure S5. The UV-vis absorption spectra of Y6 neat films with and without CN additive.

4. Device Fabrication and Characterization

The conventional structure of ITO/2PACz/Active layer/PNINN/Ag was used to fabricate the OSCs devices. The indium tin oxide (ITO) substrates were washed using ultrasonic baths by sequentially immersing the substrates in isopropanol once, detergent once, deionized water three times, and isopropanol once, each for 15 min. After dried at 70 ºC for 3 h in an oven, ITO substrates were treated with an oxygen plasma for 15 min (NovaScan UV Ozone Cleaner). Then the substrates were transferred into a nitrogen protected glove box, and coated with 2PACz at 3000 rpm for 30 s. ITO/2PACz films were annealed at 100 ºC on a hot plate in nitrogen for 10 min gave a thin film of about 10 nm. The donor PM6 and acceptor Y6 derivatives (Y6, Y6-BO, L8-BO and BTP-eC9) were kept at 1:1.2 in chloroform (CF). The total concentrations of all the blend solutions were 16 $mg \cdot mL^{-1}$. The active layer materials were dissolved after adding different solvent additives (CN, DIO, HBrT, and FBrT) to chloroform solvents (CF). The solutions were stirred at 50-100 ºC for > 1 h in a glovebox and then spin-coated on ITO/2PACz substrates, active layers with a thickness of ~ 100 nm were obtained. The active layers were deposited under vacuum for > 30 min to extract the additives (FBrT, HBrT and CN) residue before 10 min annealing at 80 ^{o}C. A 5-nm-thick PDINN layer was spun atop thereafter (1 $mg \cdot mL^{-1}$ in methanol, spin-coated at 3000 rpm for 10 s). Finally, a 100-nm-thick Ag film was deposited by thermal evaporation at a pressure of < 3×10^{-4} Pa in a glovebox to complete device fabrication.

The characteristic current-voltage (*J-V*) curves of the resulting solar cells were measured using a computer-controlled Keithley 2400 sourcemeter under 100 $mW \cdot cm^{-2}$ (1 sun, AM 1.5 G spectra, simulator provided by SAN EI, Japan) and using a mask which has an aperture with precise area of 2 mm × 2 mm (0.04 cm^2) to define the device effective area. The external quantum efficiency (EQE) measurements were carried out by using a QE-R3011 system (Enlitech, Taiwan) from 300 nm to 1000 nm.

5. Additional PV Device Performance Data

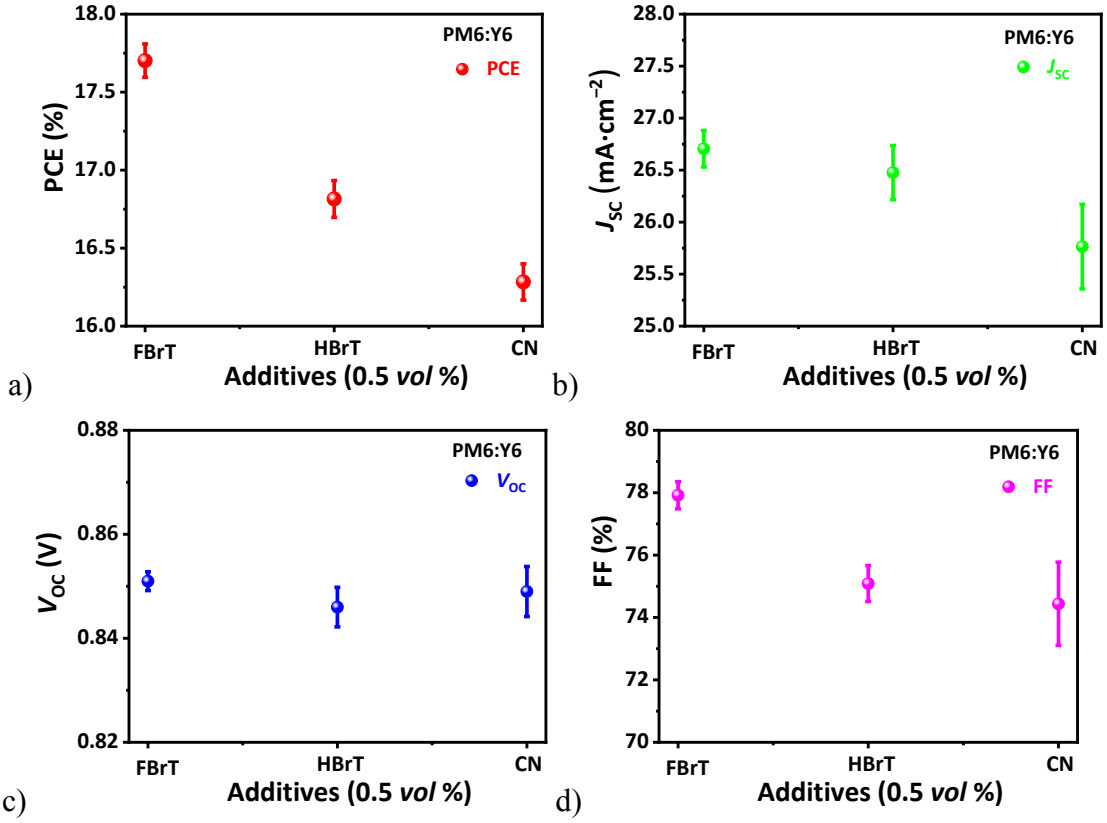

Figure S6. PCE (a); J_{SC} (b); V_{OC} (c) and FF of (d) the PM6:Y6 based BHJ polymer solar cells with different solvent additives; measurements under AM 1.5G (100 mW cm^{-2}). For each system, the markers denote the average values and error bars show the high and low values across >10 devices. Standard deviations calculated with the following Equation:

$$\sigma = \sqrt{\frac{1}{N}\sum_{i=1}^{N}(x_i - \mu)^2} \qquad (1)$$

where σ is the standard deviation, μ is the arithmetic average value of the devices' parameters, N is the total number of devices used in the determination of the standard deviations.

Table S1. Photovoltaic parameters of BHJ devices based on PM6:Y6 with different solvent additives.[a,b]

Additives (0.5 vol%)	V_{OC} (V)	J_{SC} (mA·cm^{-2})	FF (%)	PCE (%)
FBrT	0.85±0.00 (0.85)	26.7±0.2 (26.8)	77.9±0.4 (78.6)	17.7±0.1 (17.9)
HBrT	0.85±0.00 (0.85)	26.5±0.3 (26.4)	75.1±0.6 (75.9)	16.8±0.1 (17.0)
CN	0.85±0.00 (0.85)	25.8±0.4 (25.9)	74.4±1.3 (74.8)	16.3±0.1 (16.5)

[a)]Device structure: ITO/2PACz/PM6:Y6/PDINN/Ag; [b)]Average values were obtained from 10 devices under simulated AM 1.5G irradiation (100 mW cm^{-2}); Device were tested under a mask with an area of 0.04 cm^2.

Table S2. Comparison of measured J_{SC} determined from the *J*–*V* curves and integrated J_{SC} from EQE measurements.

Additives (0.5 vol%)	J_{SC}[a)] (mA cm^{-2})	J_{SC}[b)] (mA·cm^{-2})	Error (%)
FBrT	26.8	26.3	1.94
HBrT	26.4	25.8	2.33
CN	25.9	24.9	3.98

[a)]J_{SC} values determined from *J*–*V* curves; [b)]J_{SC} values calculated from EQE spectra.

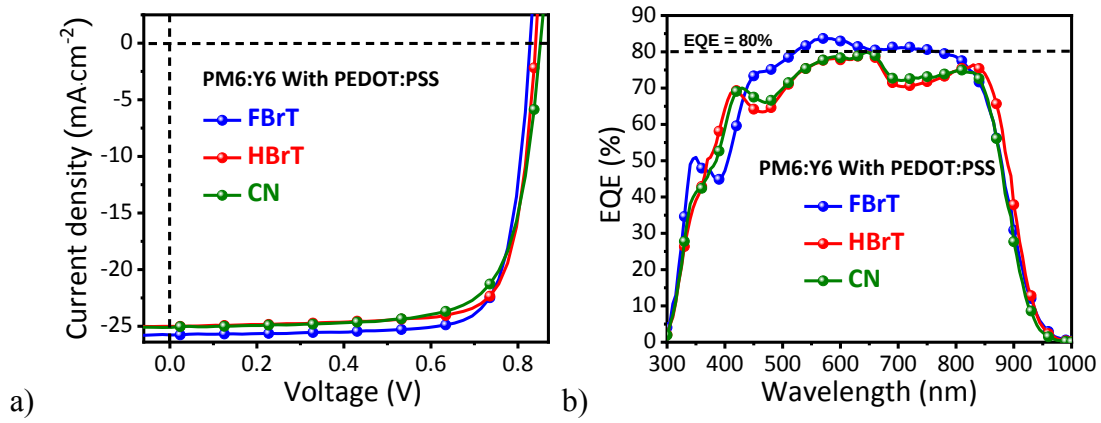

Figure S7. The (a) *J-V* curves and (b) EQE spectra curves of PM6:Y6 with different solvent additives under optimal processing parameters.

Table S3. Photovoltaic parameters of BHJ devices with different solvent additives under optimal processing parameters.[(a,b)]

Hole transport layer (HTL)	Additives (0.5 vol%)	V_{OC} (V)	J_{SC}[a)] (mA cm^{-2})	J_{SC}-EQE[b)] (mA·cm^{-2})	FF (%)	Avg. PCE (%)	Max. PCE (%)
PEDOT:PSS	FBrT	0.83	25.8	25.5	78.6	16.6	16.8
	HBrT	0.84	25.0	24.4	78.1	16.2	16.4
	CN	0.85	24.7	24.1	74.9	15.6	15.8

a) J_{SC} values determined from *J–V* curves; [b)] J_{SC} values calculated from EQE spectra.

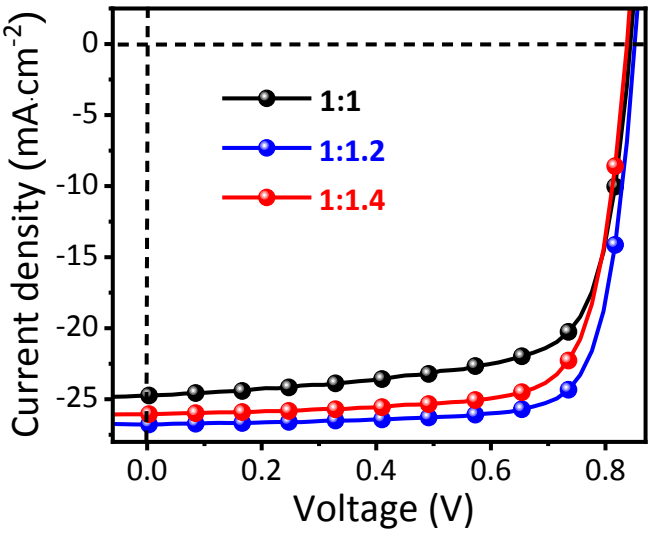

Figure S8. The *J-V* curves of PM6:Y6 based BHJ solar cells with varied D:A ratios.

Table S4. Photovoltaic parameters of PM6:Y6 based BHJ solar cells with varied D:A ratios under the illumination of AM1.5, 100 mW·cm^{-2}.

PM6:Y6 (D:A)	V_{OC} (V)	J_{SC} (mA·cm^{-2})	FF (%)	PCE (%)
1:1.1	0.84	24.0	70.4	14.2
1:1.2	0.85	26.8	78.6	17.9
1:1.4	0.84	26.1	76.2	16.6

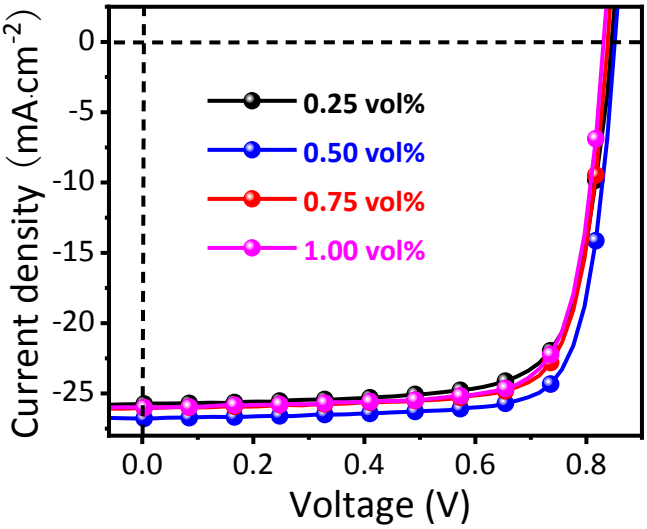

Figure S9. The *J-V* curves of PM6:Y6 based BHJ solar cells with varied contents of FBrT additive.

Table S5. Photovoltaic parameters of PM6:Y6 based BHJ solar cells with varied contents of FBrT additive.

FBrT Content (vol%)	V_{OC} (V)	J_{SC} (mA·cm^{-2})	FF (%)	PCE (%)
0.25	0.85	25.8	74.6	16.3
0.50	0.85	26.8	78.6	17.9
0.75	0.84	26.0	77.7	17.0
1.00	0.83	26.0	77.0	16.6

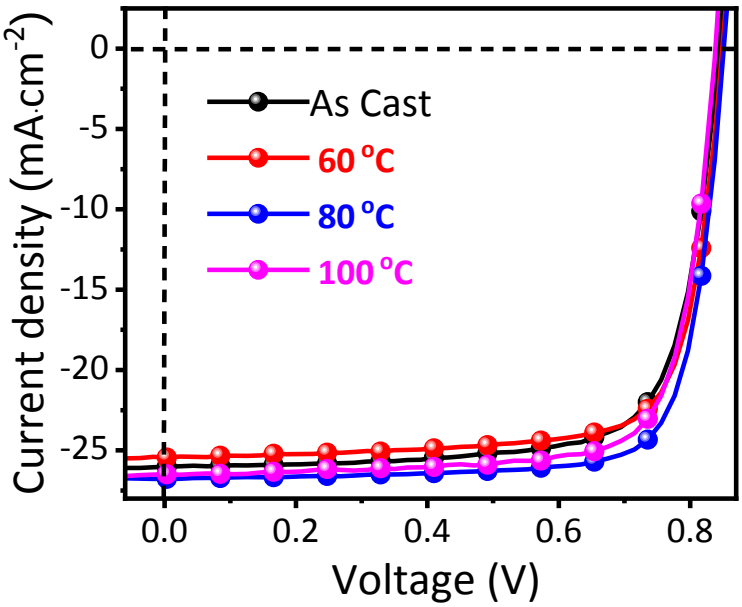

Figure S10. The *J-V* curves of PM6:Y6 based BHJ solar cells with varied thermal annealing (TA) temperatures.

Table S6. Photovoltaic parameters of PM6:Y6 based BHJ solar cells with varied thermal annealing (TA) temperatures.

TA temperature (ºC)	V_{OC} (V)	J_{SC} (mA·cm^{-2})	FF (%)	PCE (%)
As Cast	0.85	26.0	74.5	16.4
60	0.85	25.4	76.4	16.5
80	0.85	26.8	78.6	17.9
100	0.84	26.5	77.0	17.1

6. Atom Force Microscopy (AFM) Images

AFM was performed on a Multimode microscope (Veeco) by using tapping mode. The samples for AFM measurements were prepared with the structure of Quartz substrates/2PACz (10 nm) /PM6:Y6. The Quartz substrates were transferred into a nitrogen protected glove box, and coated with 2PACz at 3000 rpm for 30 s. Quartz substrates/2PACz films were annealed at 100 ºC on a hot plate in nitrogen for 10 min. The BHJ blend films were prepared by dissolving PM6:Y6 (1:1.2, wt/wt) in CF solvent and adding 0.5 vol% of different additives (FBrT, HBrT, and CN) respectively, and the total concentration of the blend solution was 16 $mg \cdot mL^{-1}$. After 3 hours of full dissolution, it was spin-coated onto Quartz substrates/2PACz films, and the BHJ blend films were tested for AFM.

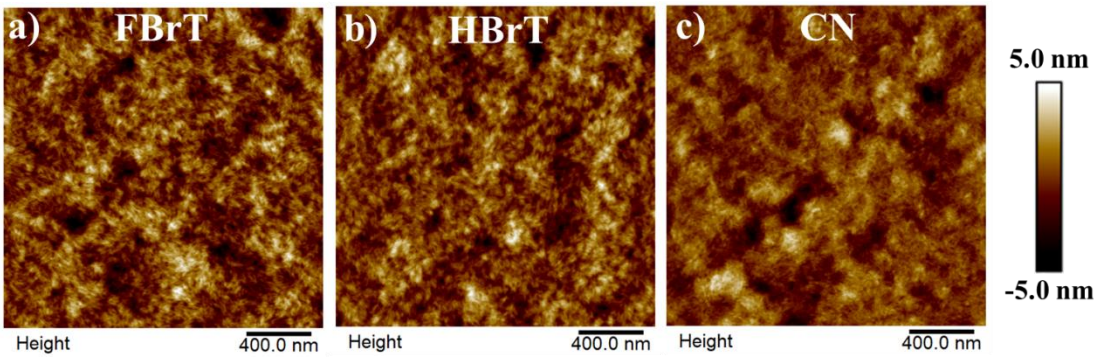

Figure S11. AFM height images of PM6:Y6 BHJ blend films with different solvent additives.

7. Transmission electron microscopy (TEM) images

Transmission electron microscopy (TEM) images were gained by applying a JEM-1400 PLUS Microscope operated at 120 kV. For TEM measurements, the sample films were firstly spun on 2PACz-coated ITO substrates and then were immersed in deionized water. Due to the water-soluble nature of 2PACz, the active layers fell off the substrates and floated up to the water surface. Copper grids with no carbon film covered were used to hold-up the floating active layers, and then these grid-held film samples were put under vacuum to evaporate the water.

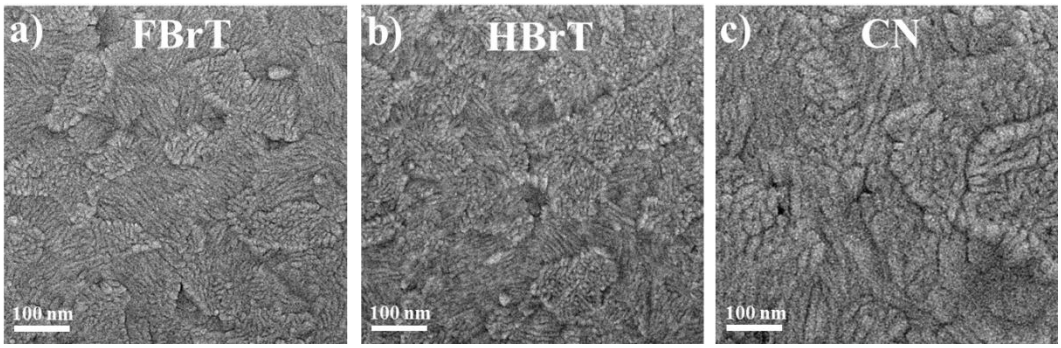

Figure S12. TEM phase images of PM6:Y6 BHJ blend films with different solvent additives.

8. Laser Confocal Raman Microspectroscopy

Raman mapping were measured by DXR2xi Raman Imaging Microscope. PM6 possesses a characteristic Raman peak at 2977 cm^{-1}, and Y6 has a characteristic Raman peak at 2220 cm^{-1}.

The Quartz substrates were transferred into a nitrogen protected glove box, and coated with 2PACz at 3000 rpm for 30 s. Quartz substrates/2PACz films were annealed at 100 ºC on a hot plate in nitrogen for 10 min. The neat films were prepared by dissolving PM6 (5 $mg \cdot mL^{-1}$) and Y6 (8 $mg \cdot mL^{-1}$) in CF solvent and adding 0.5 vol% of different additives (FBrT, HBrT, and CN) respectively. The BHJ blend films were prepared by dissolving PM6:Y6 (1:1.2, wt/wt) in CF solvent and adding 0.5 vol% of different additives (FBrT, HBrT, and CN) respectively, and the total concentration of the blend solution was 16 $mg \cdot mL^{-1}$. After 3 hours of full dissolution, it was spin-coated onto Quartz substrates/2PACz films, and the neat films and BHJ blend films were tested for Raman.

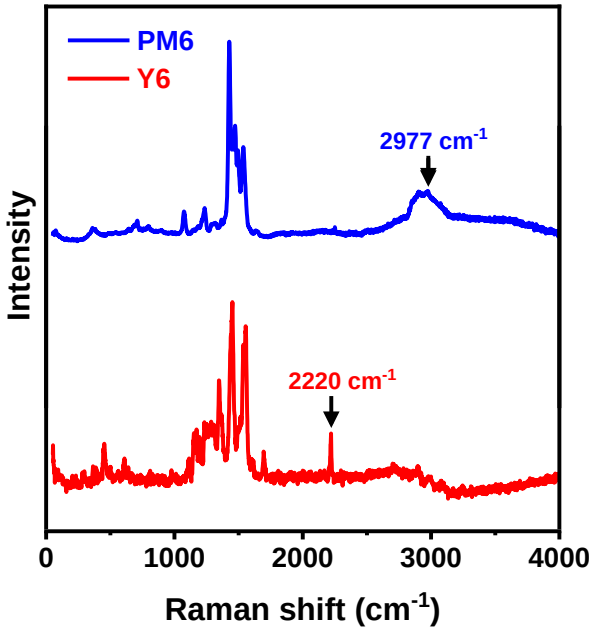

Figure S13. The Raman spectra of neat PM6 and Y6 film.

9. 2D Grazing Incidence Wide Angle X-ray Scattering (GIWAXS)

Grazing incidence wide-angle X-ray scattering (GIWAXS) characterization: GIWAXS measurements were performed at beamLine 7.3.3 at the South China University of Technology (SCUT). The 10 keV X-ray beam was incident at a grazing angle of 0.13^{o}~0.17^{o}, which maximized the scattering intensity from the samples. The scattered X-rays were detected using a Dectris Pilatus 2M photon counting detector.

The Silicon substrates were transferred into a nitrogen protected glove box, and coated with 2PACz at 3000 rpm for 30 s. Silicon substrates/2PACz films were annealed at 100 ℃ on a hot plate in nitrogen for 10 min. The neat films were prepared by dissolving PM6 (5 $mg{\cdot}mL^{-1}$) and Y6 (8 $mg{\cdot}mL^{-1}$) in CF solvent and adding 0.5 vol% of different additives (FBrT, HBrT, and CN) respectively. The BHJ blend films were prepared by dissolving PM6:Y6 (1:1.2, wt/wt) in CF solvent and adding 0.5 vol% of different additives (FBrT, HBrT, and CN) respectively, and the total concentration of the blend solution was 16 $mg{\cdot}mL^{-1}$. After 3 hours of full dissolution, it was spin-coated onto Silicon substrates, and the neat films and BHJ blend films were tested for GIWAXS.

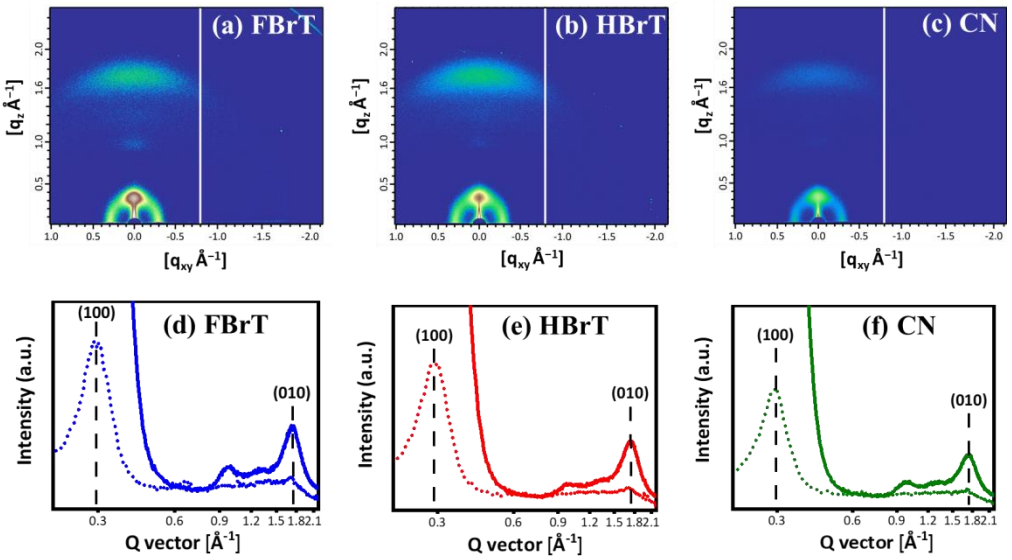

Figure S14. (a-c) The 2D GIWAXS images and (d-f) the corresponding OOP and IP line-cut profiles of neat PM6 with different solvent additives. The solid line and dotted line represent the data in OOP and IP directions, respectively.

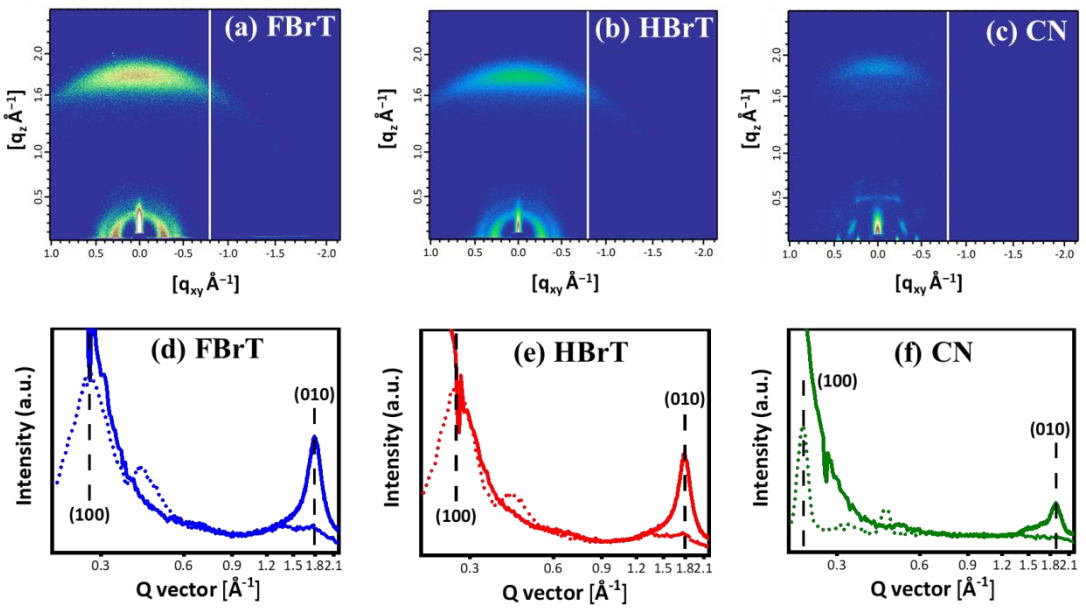

Figure S15. (a-c) The 2D GIWAXS images and (d-f) the corresponding OOP and IP line-cut profiles of neat Y6 with different solvent additives. The solid line and dotted line represent the data in OOP and IP directions, respectively.

Table S7. The detailed parameters of out-of-plane line-cut peak fitting for neat polymer donor PM6 films with different solvent additives.

Additive (0.5 vol%)	Q (Å^{-1})	Distance (Å)	FWHM (Å^{-1})	CCL[a)] (Å)
FBrT	1.72	3.65	0.20	27.64
HBrT	1.72	3.64	0.21	26.43
CN	1.74	3.60	0.23	25.08

[a)]CCL = 2πK/FWHM, in which K is the shape factor typically defined as 0.9 and FWHM is the half-width of the diffraction peak[2].

Table S8. The detailed parameters of out-of-plane peak fitting for neat acceptor Y6 films with different solvent additives.

Additive (0.5 vol%)	Q (Å^{-1})	Distance (Å)	FWHM (Å^{-1})	CCL[a)] (Å)
FBrT	1.79	3.51	0.18	31.77
HBrT	1.79	3.51	0.18	31.43
CN	1.89	3.34	0.17	34.24

[a)]CCL = 2πK/FWHM, in which K is the shape factor typically defined as 0.9 and FWHM is the half-width of the diffraction peak.

10. Exciton Dissociation and Charge Collection Efficiency

The J_{ph} is calculated by subtracting the dark current density from the current density under illumination, $J_{ph} = J_L - J_D$, in which J_L and J_D are the current density under illumination and in the dark, respectively. $V_{int} = V_{appl} - V_0$, where V_0 represents the compensation voltage when $J_{ph} = 0$, V_{appl} represents the applied bias voltage. The strength of the electric field, which is amenable to charge carrier extraction, can be described as V_{int}/L, where L represents the thickness of the active layer. As shown in Figure 6b, the J_{ph} for the optimized BHJ device (0.5 vol% FBrT) increased quickly at $V_{int} < 0.1$ V and reached saturation regime early at $V_{int} > 0.3$ V. The field-independent behaviour of J_{ph} in saturation regime points out that all the charges, which were photogenerated within the devices, can be collected efficiently at $V_{int} > 0.3$ V. As for other devices, the J_{ph} showed slightly field-dependent behaviour – an observation indicative of inefficient charge extraction.

The exciton dissociation and charge collection efficiency, which are defined by $P_{diss} = J_{SC}/J_{sat}$ and $P_{coll} = J_{power}/J_{sat}$, were measured under the short circuit condition and maximum power output point, respectively. Here, J_{sat} is the J_{ph} value at high V_{int} of over 2.0 V, where photogenerated excitons can be dissociated completely into free charge carriers and extracted efficiently by electrodes, and J_{power} is the current intensity at the maximum power point.

Table S9. Summary of exciton dissociation and charge collection efficiencies of BHJ solar devices.

Additive (0.5 vol%)	J_{SC} (mA·cm^{-2})	J_{sat} (mA·cm^{-2})	J_{power} (mA·cm^{-2})	P_{diss} [a] (%)	P_{coll} [b] (%)
FBrT	26.7	27.1	24.3	99.0	90.0
HBrT	27.0	27.3	24.0	98.8	88.0
CN	25.8	26.4	23.3	97.6	87.7

[a] $P_{diss} = \frac{Jsc}{J_{sat}}$, [b] $P_{coll} = \frac{J_{power}}{J_{sat}}$, J_{sat} is the J_{ph} value at high V_{eff} of over 2.0 V, where photogenerated excitons can be dissociated completely into free charge carriers and extracted efficiently by electrodes, and J_{power} is the current density at the maximum power point.

11. Fabrication and Characterization of SCLC Devices

Charge mobilities of BHJ photoactive layers with different solvent additives are estimated from space-charge-limited current (SCLC) method. In a SCLC device, for hole only device as the example, structure of ITO/hole transporting layer (electron blocking layer)/active layer/transporting layer (electron blocking layer) will generally be used. During the voltage sweep process in the test, only holes are allowed (barely electrons) to inject into the active layer. Similarly, electron transporting layers (hole blocking layers) are applied in electron only devices.

The device structures of the hole-only and electron-only are ITO/2PACz/PM6:Y6/MoO_3/Ag and ITO/ZnO/PM6:Y6/PDINN/Ag, respectively. The charge carrier mobilities were estimated by fitting the dark current density according to SCLC equation:

$$J = \frac{9\varepsilon_0\varepsilon_r\mu V^2}{8d^3} \quad (2)$$

where J is the current density, μ is the zero-field mobility, ε_0 is the permittivity of free space, ε_r is the relative permittivity of the material, d is the thickness of the active layer, and V is the effective voltage. The effective voltage can be obtained by subtracting the offset voltage (V_{bi}) including built-in voltage and the voltage drop from the series resistance versus the applied voltage (V_{appl}), $V = V_{appl} - V_{bi}$. The charge mobility was calculated from the slope of the $J^{1/2}$ versus V curves.

The hole mobility was measured using a hole-only device with the configuration of ITO/2PACz (10 nm)/PM6:Y6/MoO_3 (10 nm)/Ag (100 nm). The electron mobility was measured using an electron-only device with the configuration of ITO/ZnO (40 nm)/PM6:Y6/PDINN (5 nm)/Ag (100 nm). The ZnO sol-gel was obtained from stirring the solution of 1.0 g $Zn(CH_3COO)_2{\cdot}2H_2O$ in 10 mL ethylene glycol monomethyl ether and 275 μL ethylenediamine at 50 ^{O}C for 12 h. ZnO layer was spin-coated on ITO at 3000 rpm for 30 s and then annealed at 200 ^{O}C in air for 2 h. The active layers were prepared following the same procedures used to fabricate the photovoltaic devices.

The hole and electron mobilities were calculated by fitting the dark current to the model of a single-carrier space charge limited current (SCLC), which is described by the MOTT-Gurney Equation (3)[3, 4]

$$J = \frac{9\varepsilon_0\varepsilon_r\mu V^2}{8L^3} \tag{3}$$

where J is the current measured under dark condition for hole-only and electron-only devices, μ is the zero-filed mobility, and ε_0 is the vacuum permittivity (ε_0 = 8.85 $C\cdot V^{-1}\cdot s^{-1}$), ε_r is the relative permittivity (for organics and polymers, ε_r is assumed to be 3.0), L is the thickness of the active layer. V is the effective internal voltage, and $V = V_{appl} - V_{bi} - V_s$, V_{appl} is the applied voltage, V_{bi} is the built-in voltage induced by the work function difference of the two electrodes and V_s is the voltage drop from the substrate's series resistance (for electron-only device, V_s = 0 V, while for hole-only device, the series resistance is assumed to be 10 Ω which is caused by MoO_3 layer). Then the mobilities can be extracted from the slope of the $J^{1/2} - V$ curves by the Equation (4):

$$\mu = \frac{\text{slope}^2 \times 8L^3}{9\varepsilon_0\varepsilon_r} \tag{4}$$

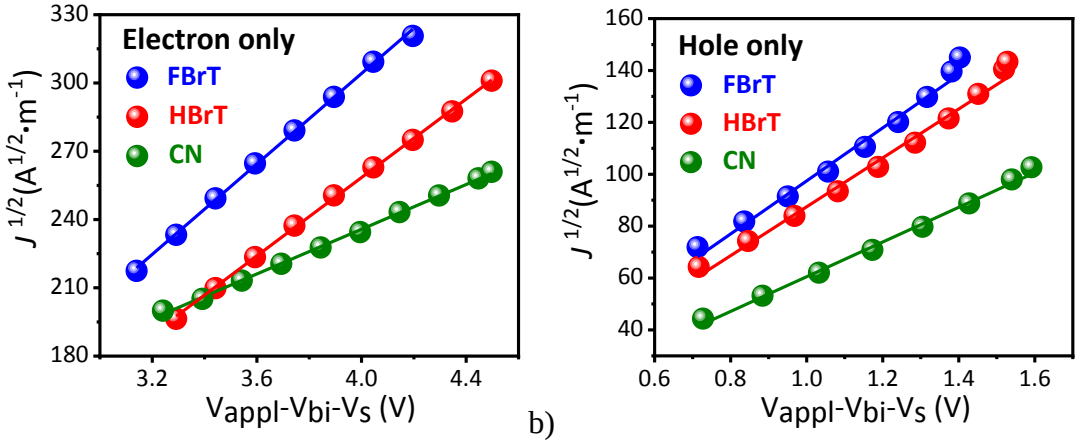

Figure S16. Dark *J-V* characteristics of (a) electron-only and (b) hole-only diodes made with PM6:Y6 BHJ blend films. The experimental data are fitted using the carrier SCLC model (solid lines).

Table S10. Summary of hole and electron mobilities extracted from SCLC fittings shown in Figure S16.

Additive (0.5 vol%)	μ_h ($\times10^{-3}$ $cm^2 \cdot V^{-1} \cdot s^{-1}$)	μ_e ($\times10^{-3}$ $cm^2 \cdot V^{-1} \cdot s^{-1}$)	μ_h/μ_e
FBrT	3.49	3.30	1.06
HBrT	2.86	2.39	1.20
CN	1.34	0.72	1.86

[a)]Hole-only device structure: ITO/2PACz/PM6:Y6/MoO_3/Ag.

[b)]Electron-only device structure: ITO/ZnO/PM6:Y6/PNINN/Ag.

12. Photovoltaic Performance of PM6:LB-BO with Solvent Additives

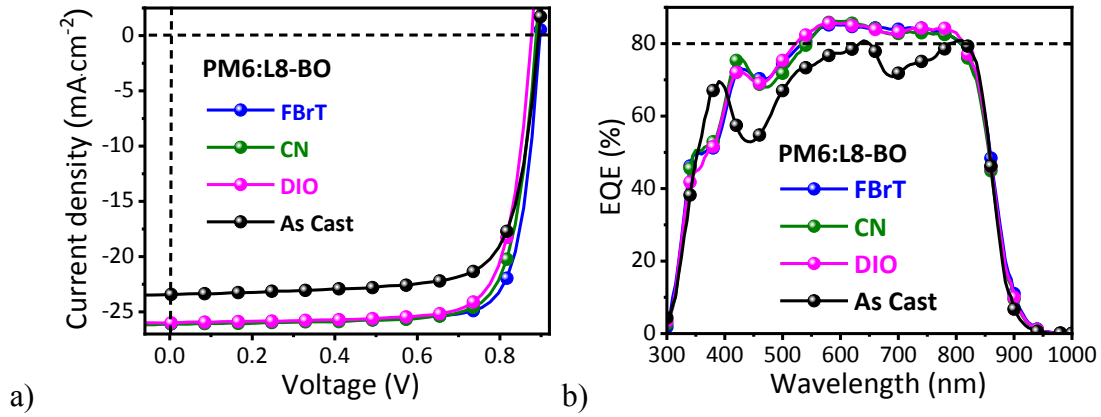

a) b)

Figure S17. (a) The *J*-*V* curves and (b) EQE spectra of PM6:L8-BO with different solvent additives.

Table S11. Photovoltaic parameters of BHJ devices based on PM6:L8-BO with different solvent additives.[(a,b)]

Additives (0.5 vol%)	V_{OC} (V)	J_{SC}[c)] (mA cm^{-2})	J_{SC}-EQE[d)] (mA cm^{-2})	Error (%)	FF (%)	Avg. PCE (%)	Max. PCE (%)
FBrT	0.90	25.9	25.2	2.78	80.1	18.6	18.7
CN	0.89	26.1	25.3	3.12	78.4	17.9	18.2
DIO	0.88	26.0	25.2	3.26	77.8	17.3	17.7
As Cast	0.89	23.4	22.9	2.18	75.3	15.1	15.8

[a)]Device structure: ITO/2PACz/PM6:L8-BO/PDINN/Ag; [b)]Average values were obtained from 10 devices under simulated AM 1.5G irradiation (100 mW cm^{-2}), device were tested under a mask with an area of 0.04 cm^2; [c)]J_{SC} values determined from *J*–*V* curves; [d)]J_{SC} values calculated from EQE spectra.

13. Photovoltaic Performance of PM6:Y6-BO with Solvent Additives

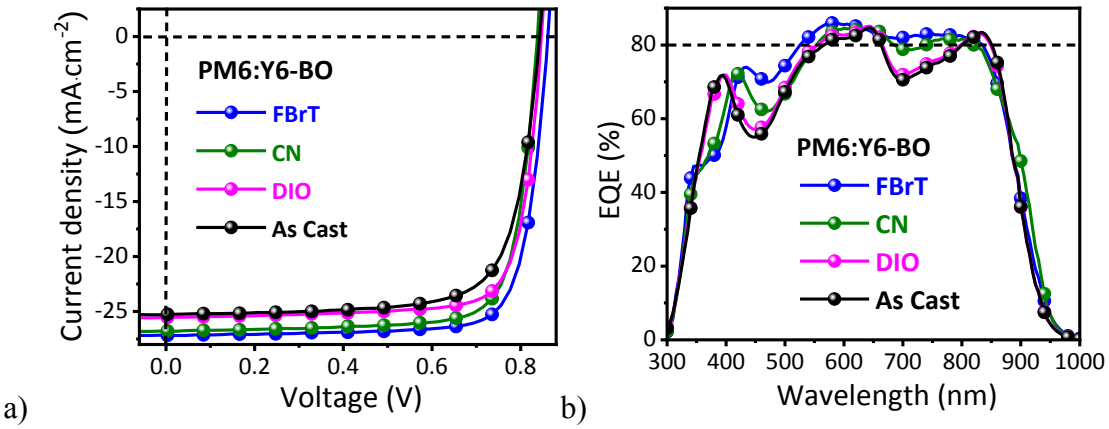

Figure S18. (a) The *J-V* curves and (b) EQE spectra of PM6:Y6-BO with different solvent additives.

Table S12. Photovoltaic parameters of BHJ devices based on PM6:Y6-BO with different solvent additives.[a,b]

Additives (0.5 vol%)	V_{OC} (V)	J_{SC}[c] (mA cm^{-2})	J_{SC}-EQE[d] (mA cm^{-2})	Error (%)	FF (%)	Avg. PCE (%)	Max. PCE (%)
FBrT	0.86	27.2	26.5	2.45	79.3	18.3	18.6
CN	0.84	26.8	26.0	3.12	78.4	17.4	17.6
DIO	0.85	25.5	25.2	1.26	78.3	16.5	17.0
As Cast	0.84	25.3	25.0	1.20	74.3	15.2	15.8

[a]Device structure: ITO/2PACz/PM6:Y6-BO/PDINN/Ag; [b]Average values were obtained from 10 devices under simulated AM 1.5G irradiation (100 mW cm^{-2}), device were tested under a mask with an area of 0.04 cm^2; [c]J_{SC} values determined from *J–V* curves; [d]J_{SC} values calculated from EQE spectra.

14. Photovoltaic Performance of PM6:BTP-eC9 with Solvent Additives.

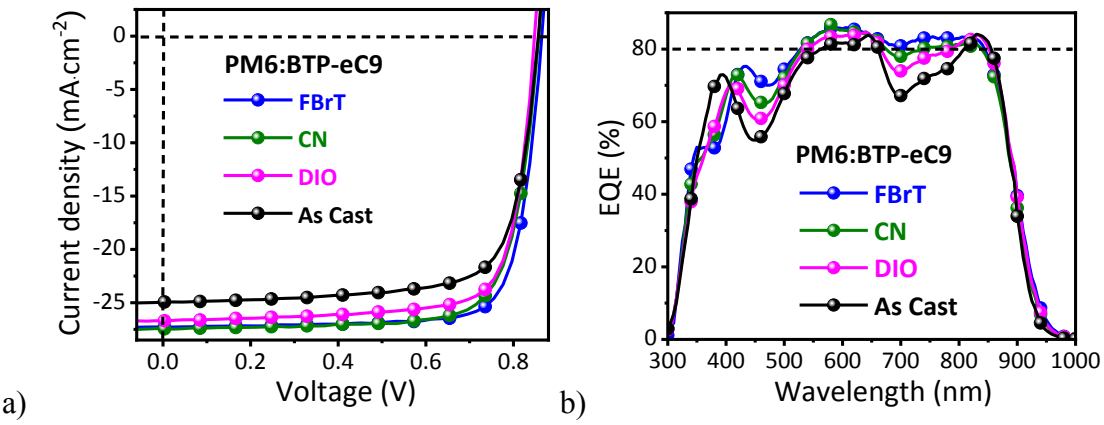

a) b)

Figure S19. (a) The *J-V* curves and (b) EQE spectra of PM6:BTP-eC9 with different solvent additives.

Table S13. Photovoltaic parameters of BHJ devices based on PM6:BTP-eC9 with different solvent additives.[(a,b)]

Additives (0.5 vol%)	V_{OC} (V)	J_{SC}[c)] (mA cm^{-2})	J_{SC}-EQE[d)] (mA cm^{-2})	Error (%)	FF (%)	Avg. PCE (%)	Max. PCE (%)
FBrT	0.87	27.3	26.7	1.61	78.9	18.5	18.7
CN	0.86	27.4	26.4	4.14	76.4	17.7	18.0
DIO	0.85	26.7	25.7	3.70	77.2	17.2	17.5
As Cast	0.86	24.9	24.7	0.81	74.6	15.0	15.9

[a)]Device structure: ITO/2PACz/PM6:BTP-eC9/PDINN/Ag; [b)]Average values were obtained from 10 devices under simulated AM 1.5G irradiation (100 mW cm^{-2}), device were tested under a mask with an area of 0.04 cm^2; [c)]J_{SC} values determined from *J*–*V* curves; [d)]J_{SC} values calculated from EQE spectra.

15. Solution NMR Spectra of Solvent Additive FBrT.

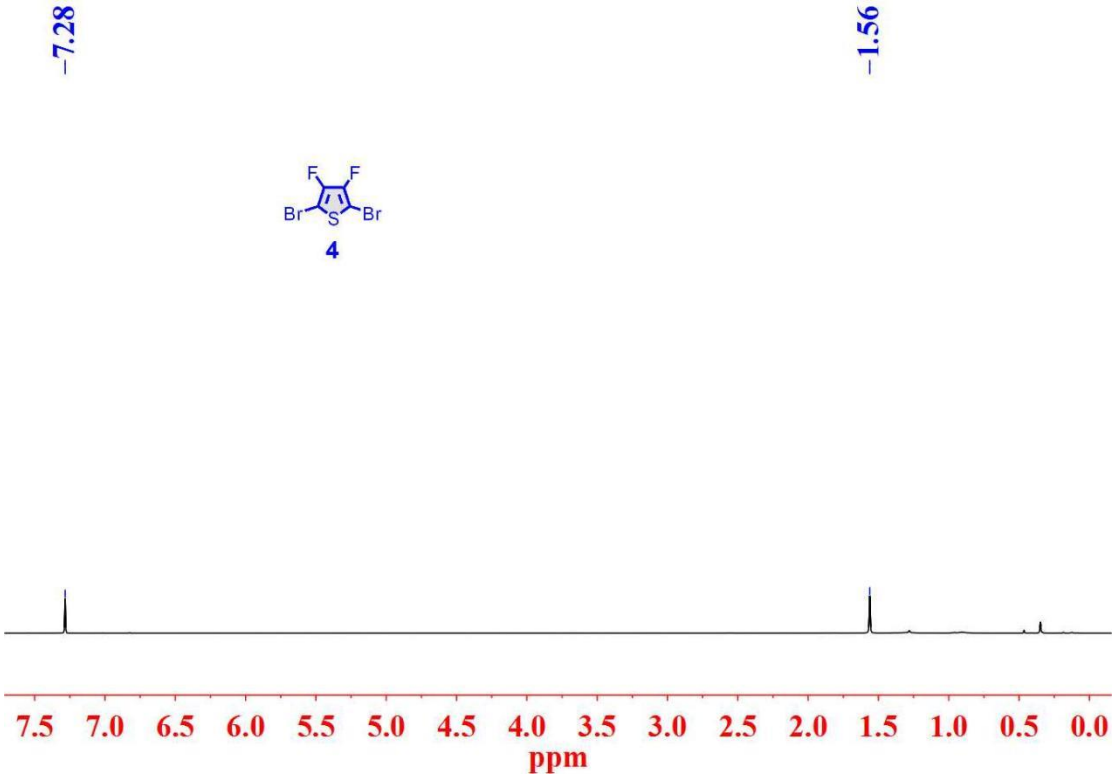

Figure S20. The ^{1}H NMR spectrum of FBrT in $CDCl_3$.

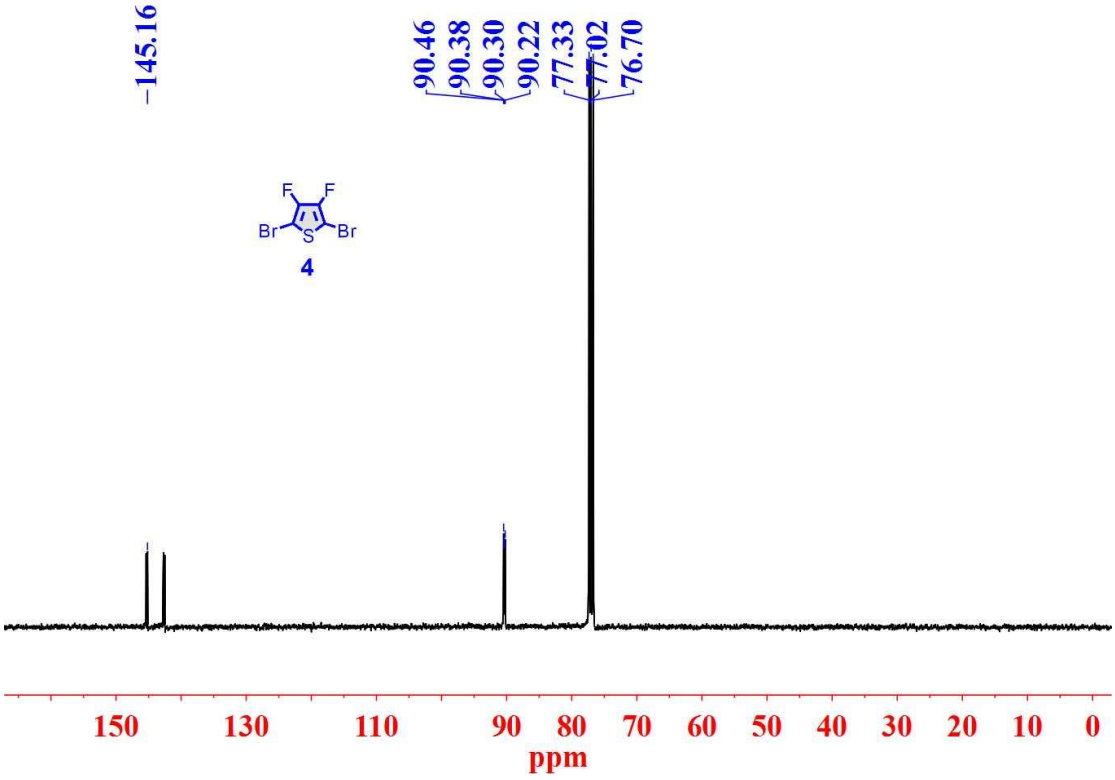

Figure S21. The ^{13}C NMR spectrum of FBrT in $CDCl_3$.

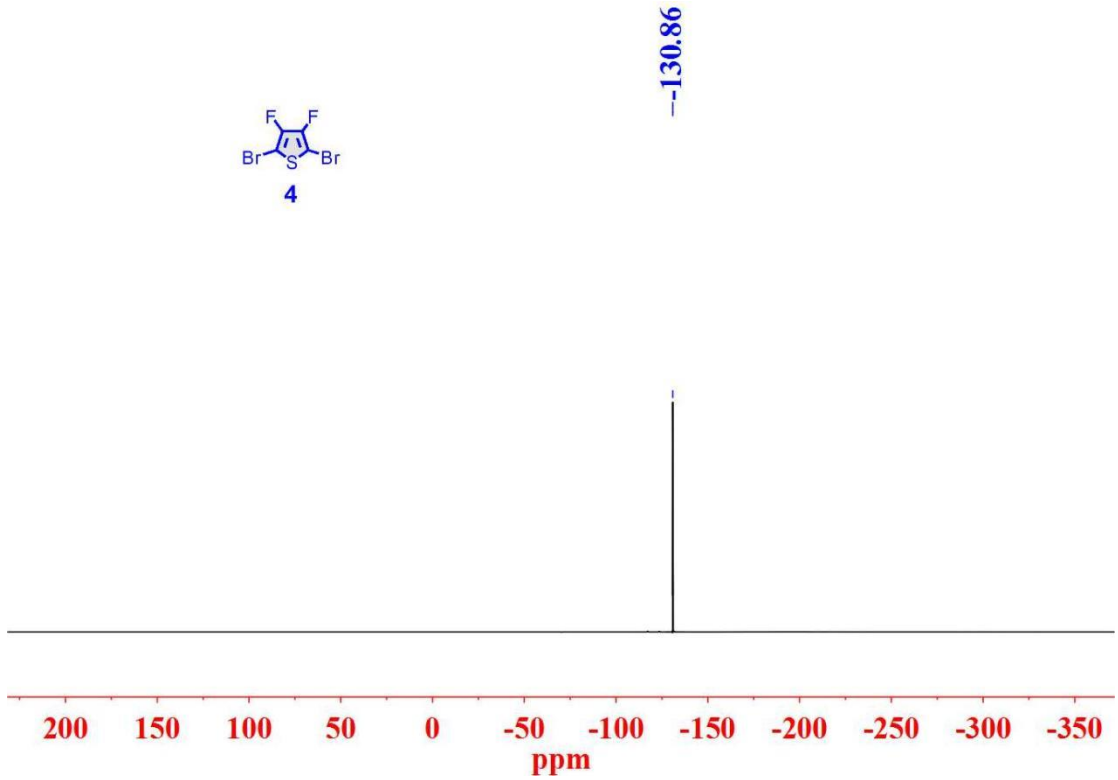

Figure S22. The ^{19}F NMR spectrum of FBrT in $CDCl_3$.

16. Supporting Information References

1. S. Liu, Y. Firdaus, S. Thomas, Z. Kan, F. Cruciani, S. Lopatin, J. Bredas and P. M. Beaujuge, *Angew. Chem. Int. Ed.*, 2018, **57**, 531-535.
2. K. Kawashima, T. Fukuhara, Y. Suda, Y. Suzuki, T. Koganezawa, H. Yoshida, H. Ohkita, I. Osaka and K. Takimiya, *J. Am. Chem. Soc.*, 2016, **138**, 10265-10275.
3. Z. Li, K. Jiang, G. Yang, J. Y. L. Lai, T. Ma, J. Zhao, W. Ma and H. Yan, *Nat. Commun.*, 2016, **7**, 13094.
4. P. Blom, M. J. M. De Jong and M. G. Van Munster, *Physical Review B*, 1997, **55**, R656-R659.